

# Quantitative Characterization of Interface Traps in Ferroelectric/Dielectric Stack Using Conductance Method

Yiming Qu<sup>ID</sup>, Student Member, IEEE, Junkang Li, Member, IEEE, Mengwei Si<sup>ID</sup>, Member, IEEE, Xiao Lyu, Student Member, IEEE, and Peide D. Ye<sup>ID</sup>, Fellow, IEEE

**Abstract**—In this work, the conductance method with an optimized circuit model is established to investigate the trapped charges at the ferroelectric/dielectric (FE/DE) interface. The density of interface states is quantitatively characterized to be  $\sim 4 \times 10^{12}$  to  $10^{13} \text{ cm}^{-2} \cdot \text{eV}^{-1}$ . And the injection and accumulation of these enormous interfacial charges play a key role in the operation of the FE/DE stack. The proposed measurement technique provides a comprehensive understanding of the FE/DE stack as well as some new insights of negative capacitance effect and ferroelectric field-effect transistor device operations.

**Index Terms**—Conductance method, ferroelectric/leakage (FE/DE), hafnium zirconium oxide, interface traps, leakage-assist-switching mechanism.

## I. INTRODUCTION

FERROELECTRIC-GATED field-effect transistor (FET) has been extensively studied for several years for its application on nonvolatile memory as ferroelectric FET (Fe-FET) [1]–[5]. The proposal of negative capacitance (NC) effect in ferroelectric devices exploits the development of NC-FET for low-power CMOS logic due to the steep sub-threshold swing below 60 mV/decade [6]–[10]. No matter in Fe-FETs or NC-FETs, the ferroelectric/dielectric (FE/DE) stack is commonly applied, where the DE layer is inevitable in the form of native oxide or passivation layer for a substrate. Therefore, the study of the FE/DE stack is of great

Manuscript received July 26, 2020; revised October 13, 2020 and October 19, 2020; accepted October 22, 2020. Date of publication November 16, 2020; date of current version November 24, 2020. This work was supported in part by the Applications and Systems-driven Center for Energy-Efficient Integrated Nano Technologies (ASCENT), one of six Centers in the Joint University Microelectronics Program (JUMP), a Semiconductor Research Corporation (SRC) Program sponsored by DARPA, and in part by the Air Force Office of Scientific Research. This article was originally presented in the 2020 Virtual Symposium on VLSI Technology. The review of this article was arranged by Editor M. Kobayashi. (Corresponding author: Peide D. Ye.)

Yiming Qu and Junkang Li are with the Birck Nanotechnology Center, School of Electrical and Computer Engineering, Purdue University, West Lafayette, IN 47907 USA, and also with the College of Electronic Engineering and Information Science, Zhejiang University, Hangzhou 310027, China.

Mengwei Si, Xiao Lyu, and Peide D. Ye are with the Birck Nanotechnology Center, School of Electrical and Computer Engineering, Purdue University, West Lafayette, IN 47907 USA (e-mail: yep@purdue.edu).

Color versions of one or more figures in this article are available at <https://doi.org/10.1109/TED.2020.3034564>.

Digital Object Identifier 10.1109/TED.2020.3034564

importance. It is well-known that the FE/DE stack is fundamentally different from an FE capacitor and a DE capacitor in series [12], [13]. It becomes complicated due to the FE/DE interfacial coupling effect and charge accumulation at the FE/DE interface [14]–[22]. It is a fact that there is a gap of charge mismatch between remnant polarization in FE layers and maximum tolerable charge density in DE layers [18]. The remnant polarization  $P_r$  of typical ferroelectric films is at the order of  $10 \mu\text{C}/\text{cm}^2$ , whereas conventional dielectric insulators cannot support such a large charge density unless the existence of large leakage current and eventually the breakdown of dielectric. Thus, the leakage current and interfacial charges at the FE/DE interface are the only possible mechanism to make the polarization switching happen possible to satisfy the charge balance requirement [18]. In addition, the degradation of FeFETs has also been reported to be dominantly impacted by the interface properties, which is indicative of the significant FE/DE interfacial behavior during the operation of FE/DE stack [22]–[24]. However, the FE/DE interface trap properties have not been intensively and quantitatively investigated thoroughly.

Recently, a simultaneous  $I_d$ – $V_g$  and polarization-voltage ( $P$ – $V$ ) measurements by the positive up negative down (PUND) pulse was applied to Fe-FETs to extract the defect density of interface [23]. By calculating the undesired non-ferroelectric hysteresis loop of  $I_d$ – $V_g$  curves, a charge density of  $\sim 10^{13} \text{ cm}^{-2}$  at the FE/DE interface was obtained, which accounts for the stress-induced imprint voltage shift in the  $P$ – $V$  loops. The charge density from this method is independent of polarization switching. Another novel split  $C$ – $V$  technique combined with Hall measurement has been introduced to separate interface traps from the ferroelectric polarization charges in Fe-FETs, shown a surprisingly large trapped charge of  $\sim 10^{14} \text{ cm}^{-2}$  as the key role in the performance-boosting of transistors [20]. Nonetheless, the semiconductor/DE interface is also involved in the Fe-FETs, and the charge trapping at the semiconductor/DE interface might be confused with that at the FE/DE interface. To make the study of the FE/DE interface more distinct and straightforward, an FE/DE capacitor is more preferable.

In this work, the charge behaviors and interface trap properties at the FE/DE interface are quantitatively characterized in the structure of metal/FE/DE/metal capacitor. Hafnium

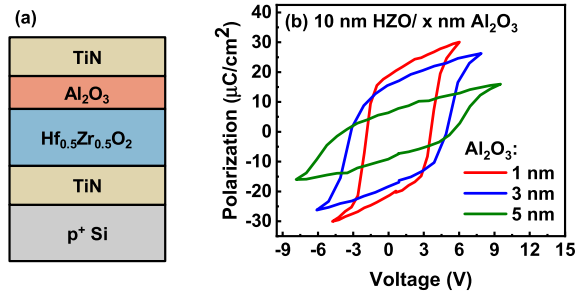


Fig. 1. (a) Cross section structure of the fabricated HZO/ $\text{Al}_2\text{O}_3$  capacitor. (b)  $P$ - $V$  hysteresis loops of the HZO/ $\text{Al}_2\text{O}_3$  capacitors with 10-nm HZO and different  $\text{Al}_2\text{O}_3$  thicknesses of 1, 3, and 5 nm.

zirconium oxide ( $\text{Hf}_{0.5}\text{Zr}_{0.5}\text{O}_2$ , HZO) is chosen as the FE layer and high- $k$  insulator  $\text{Al}_2\text{O}_3$  is chosen as the DE layer.  $P$ - $V$  and  $C$ - $V$  properties are first measured to examine the existence of interface traps. Then, the conductance method, which is widely used for the study of the metal-oxide-semiconductor (MOS) interface [25], is formulated to measure the trap density at the FE/DE interface ( $D_{it}$ ). Our previous work [21] reported the conductance peak phenomenon in FE/DE stack in  $C$ - $V$  measurement. In this work, taking the consideration of leakage current through FE/DE stack and band bending fluctuation effect into the circuit and mathematical model for an accurate characterization of FE/DE interface trap behaviors are developed based on the main results of [21]. Using this optimized model, a distribution of  $D_{it}$  and the corresponding time constant  $\tau_{it}$  at different polarization states are finally extracted at different temperatures. It is found that the charge trapping at the FE/DE interface, which is supplied from the leakage currents through the ultrathin DE layer, dominates the polarization switching of FE/DE stack.

## II. EXPERIMENTS

### A. Capacitor Fabrication

Metal/FE/DE/metal capacitors were fabricated for the investigation of the FE/DE interface, as the cross-sectional schematic shown in Fig. 1(a). Heavily p-doped Si wafers with the resistivity less than  $0.005 \Omega \cdot \text{cm}$  were adopted as the substrate after standard solvent cleaning. As the metal contact, TiN was deposited by atomic layer deposition (ALD) at  $250^\circ\text{C}$ , using the  $[(\text{CH}_3)_2\text{N}]_4\text{Ti}$  and  $\text{NH}_3$  as the Ti and N precursors, respectively. Alternating monolayers of  $\text{HfO}_2$  and  $\text{ZrO}_2$  were deposited by ALD at  $200^\circ\text{C}$  to achieve an overall film composition of  $\text{Hf}_{0.5}\text{Zr}_{0.5}\text{O}_2$  and a thickness of 10 nm, using  $[(\text{CH}_3)_2\text{N}]_4\text{Hf}$ ,  $[(\text{CH}_3)_2\text{N}]_4\text{Zr}$  and  $\text{H}_2\text{O}$  as the precursors of Hf, Zr, and O, respectively. To avoid cross-contamination, the TiN and HZO films were deposited in two separate chambers, which are connected externally by the Ar environment in a glove box to avoid environmental contamination. Next, the stacked  $\text{Al}_2\text{O}_3$  layer with three different thicknesses (1, 3, 5 nm) was deposited by ALD at  $200^\circ\text{C}$ , using  $(\text{CH}_4)_3\text{Al}$  and  $\text{H}_2\text{O}$  as the Al and O precursors. Another TiN layer was deposited on the top of the HZO/ $\text{Al}_2\text{O}_3$  stack. Both the bottom and top TiN films are metallic and have the same thickness of 30 nm. After deposition, all samples were annealed at  $500^\circ\text{C}$  in the  $\text{N}_2$  environment for 1 min by rapid

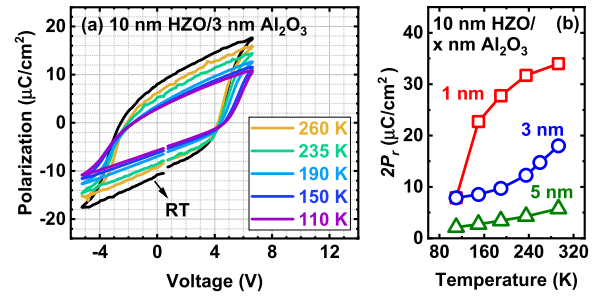


Fig. 2. (a)  $P$ - $V$  hysteresis loops of the 10-nm HZO/3-nm  $\text{Al}_2\text{O}_3$  capacitor at low temperatures from RT to 110 K. (b) Temperature dependence of  $P_r$  for the HZO/ $\text{Al}_2\text{O}_3$  capacitor with different  $\text{Al}_2\text{O}_3$  thicknesses.

thermal annealing to crystallize the HZO film. Then, Ti/Au top electrodes were fabricated by photolithography, e-beam evaporation, and a liftoff process. Dry etching was used to remove the top TiN layer by  $\text{CF}_4/\text{Ar}$ .

### B. Electrical Characterization

Electrical characterizations at room temperature (RT) were probed in a Cascade summit probe station and low temperature experiments were conducted in a Lakeshore cryogenic probe station. The capacitance-voltage ( $C$ - $V$ ) and conductance measurements were taken using an Agilent E4980A impedance analyzer and  $P$ - $V$  measurements were carried out using a Radiant RT66 ferroelectric tester. The applied voltage ranges were maximized in  $P$ - $V$  measurements before the leakage current had essential impacts. All devices have already been woken up before the  $P$ - $V$  characterization.

## III. RESULTS AND DISCUSSION

### A. Temperature-Dependent $P$ - $V$ and $C$ - $V$ Properties

Fig. 1(b) shows the  $P$ - $V$  curves of the HZO/ $\text{Al}_2\text{O}_3$  capacitors with 10-nm HZO and different  $\text{Al}_2\text{O}_3$  thicknesses from 1 to 5 nm. The ferroelectric hysteresis loops are observed which confirms the ferroelectricity of these HZO/ $\text{Al}_2\text{O}_3$  capacitors. It is also found that the remnant polarization ( $P_r$ ) decreases with the increasing  $\text{Al}_2\text{O}_3$  thickness, which is due to the leakage-assist-switching mechanism [18]. The leakage currents through ultrathin  $\text{Al}_2\text{O}_3$  layers with different thicknesses supply different quantities of mismatched charges for polarization switching, thus resulting in different  $P_r$ . These mismatched charges are essentially the trapped charges at the FE/DE interface.

To further demonstrate and investigate this charge trapping process, temperature-dependent  $P$ - $V$  measurements were performed. Fig. 2(a) shows the  $P$ - $V$  hysteresis loops for the 10-nm HZO/3-nm  $\text{Al}_2\text{O}_3$  capacitor at low temperatures from 110 K to RT of 293 K. Temperature-dependent  $P_r$  is summarized in Fig. 2(b) for capacitors with different  $\text{Al}_2\text{O}_3$  thickness.  $P_r$  decreases with the decreasing temperature, indicating the suppression of polarization switching. This phenomenon is the result of leakage current reduction through  $\text{Al}_2\text{O}_3$  and the suppression of trap response at low temperatures, resulting in fewer trapped charges for polarization switching. It also indicates that the leakage-assist charge injection through the

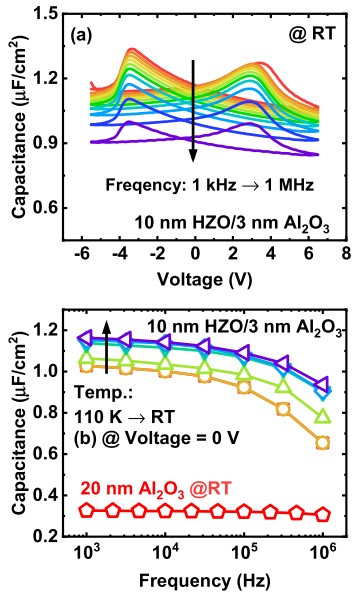


**Fig. 3.** (a) Frequency dispersion of  $C-V$  properties for the 10-nm HZO/3-nm  $\text{Al}_2\text{O}_3$  capacitor measured from 1 kHz to 1 MHz. (b) Frequency-dependent capacitance at zero bias voltage for the 10-nm HZO/3-nm  $\text{Al}_2\text{O}_3$  capacitor measured from RT to 110 K. The capacitor with 20-nm  $\text{Al}_2\text{O}_3$  in red is shown as the control sample.

FE/DE stack contains not only tunneling current but also thermionic emission process [26], [27]. Polarization switching at cryogenic temperatures suggests that both direct tunneling and trap-assisted tunneling are associated with the electron transport. Furthermore,  $P_T$  is found to decrease much more quickly in capacitors with thinner  $\text{Al}_2\text{O}_3$ , suggesting that thermionic emission contributes sufficiently to the leakage current transport.

$C-V$  characteristics were also measured at different frequencies and different temperatures. The frequency-dependent  $C-V$  properties, ranging from 1 kHz to 1 MHz at RT, are shown in Fig. 3(a) for 10-nm HZO/3-nm  $\text{Al}_2\text{O}_3$  capacitor. The capacitance decreases with the increasing frequency, as fewer traps respond to a higher frequency. The control sample, a capacitor with 20-nm  $\text{Al}_2\text{O}_3$  dielectric layer only was also measured and its capacitance value keeps almost constant at the whole frequency regime, as the red symbols and line shown in Fig. 3(b). Therefore, this frequency dispersion is not induced by the measurement setup or parasitic effect. Fig. 3(b) shows the frequency-dependent capacitance value at low temperatures from RT down to 110 K. A smaller capacitance and larger frequency dispersion are observed at lower temperatures, which is attributed to the suppression of trap responses and charge injection. All these  $P-V$  and  $C-V$  measurement results under various temperatures and frequencies manifest the charge trapping at the FE/DE interface, supplied from leakage currents through the ultrathin DE layer, which is critical for the charge balance and polarization switching of FE HZO eventually.

### B. Principle of Conductance Method for FE/DE Stack

The conductance method, proposed by Nicollian and Goetzberger [25], is a sensitive technique to determine the trap density at the MOS interface. As a loss mechanism,

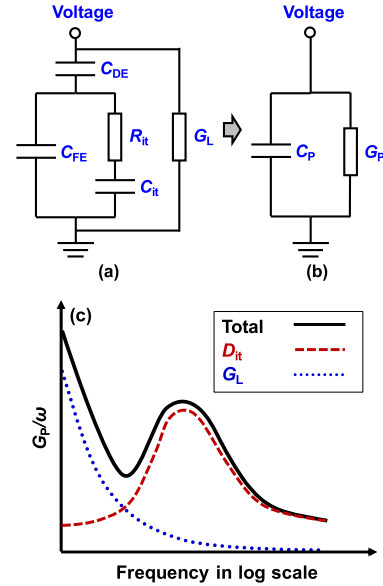


**Fig. 4.** (a) Equivalent circuit model for the conductance method applied to the FE/DE stack after considering the leakage current through the FE/DE stack. (b) Simplified equivalent circuit model for the conductance measurement by impedance analyzers. (c) Schematic of the  $G_p/\omega$  and its components. The red dashed line and blue dotted line represent the interface trap-related  $D_{it}$  item and leakage current-related  $G_L$  term in (2), respectively. As a result, the black solid line shows an example of the conductance curve of FE/DE capacitors for the extraction of  $D_{it}$  and  $\tau_{it}$ .

interface trap capture and emission of carriers are represented by the conductance. This trap resulted loss process, as well as capacitances in the MOS structure, are lumped to the parallel of an equivalent conductance and an equivalent capacitor. By applying a series of small-signal sine waves with different frequencies, this equivalent parallel conductance is measured, then the interface trap density and time constant can be obtained by fitting the measurement results to a theoretical circuit model. Comparing the possible equivalent circuit model of FE/DE stack with that MOS capacitor, the conductance method can also be applied to extract properties of the FE/DE interface traps.

Fig. 4(a) shows the proposed equivalent circuit of FE/DE stack, which is similar to that of MOS capacitors. The branch, including interface trap-related resistance  $R_{it}$  and capacitance  $C_{it}$ , is parallelly connected with the FE capacitance  $C_{FE}$  and then connected with the DE capacitance  $C_{DE}$  in series. Here, the interaction of interface traps with polarization charges by  $D_{it}$  ( $C_{it} = qD_{it}$ ) is a lossy process, represented by  $R_{it}$ . A conductance component  $G_L$  is introduced because of the leakage currents through the FE/DE stack. It will not affect the measurement result of interface traps, which will be explained later.

Because the impedance analyzers generally assume the device under test to consist of the parallel of measured conductance  $G_p$  and measured capacitance  $C_p$ , one can replace the circuit of Fig. 4(a) by that in Fig. 4(b) for convenience, assuming negligible series resistance in the system. Thus, the total admittance  $Y_{it}$  of Fig. 4(a) can be normalized into the parallel connection of conductance  $G_p$  and capacitance  $C_p$  with

$$Y_{it} = G_p + j\omega C_p \quad (1)$$

and

$$\frac{G_P}{\omega} = \frac{(\omega\tau_{it})C_{DE}^2C_{it}}{(\omega\tau_{it})^2(C_{FE} + C_{DE})^2 + C_A^2} + \frac{G_L}{\omega} \quad (2)$$

$$C_P = \frac{C_A C_{FE}(C_{it} + C_{DE}) + (\omega\tau_{it})^2 C_{FE} C_{DE}(C_{FE} + C_{DE})}{(\omega\tau_{it})^2(C_{FE} + C_{DE})^2 + C_A^2} \quad (3)$$

where  $\omega$  is proportional to the measurement frequency  $f$ , and  $\tau_{it}$  is equal to  $R_{it}C_{it}$ . Here, for a clear description,  $C_A$  is the sum of all capacitances, defined as

$$C_A = C_{FE} + C_{DE} + C_{it}. \quad (4)$$

To demonstrate the validity of this circuit model, the component of  $C_P$  is analyzed first. It can be expressed as (5) when extending  $\omega$  to zero and as (6) when to infinity

$$C_P = \frac{C_{DE}(C_{FE} + C_{it})}{C_{FE} + C_{DE} + C_{it}} (\omega \rightarrow 0) \quad (5)$$

$$C_P = \frac{C_{DE}C_{FE}}{C_{FE} + C_{DE}} (\omega \rightarrow \infty). \quad (6)$$

It is found that  $C_P$  is the serial connection of  $C_{DE}$  and  $C_{FE}$  at high frequency. However, at low frequency,  $C_P$  includes an extra branch of  $C_{it}$  in parallel with  $C_{FE}$ . This changing tendency of  $C_P$  is consistent with the measurement result in Fig. 3(b), which can be theoretically explained by the frequency-related trap responses. The interface traps can respond to low-frequency signals but lag at high frequency. On the other hand, it is confirmed that for capacitors of 10-nm HZO/3-nm  $Al_2O_3$ , the numerical calculated  $C_P$  at RT, using (6) with the real  $C_{DE}$  ( $\sim 1.9 \mu F/cm^2$ ) and  $C_{FE}$  ( $\sim 2.3 \mu F/cm^2$ ), is approximate to the measured  $0.95 \mu F/cm^2$  as shown in Fig. 3(b). In addition, for all the measured devices with different  $Al_2O_3$  thicknesses, the numerical calculated  $C_P$  using (6) with the real  $C_{DE}$  and  $C_{FE}$  have been confirmed to be approximate to the measured capacitance value at 1 MHz. Both phenomena indicate that the application of the conductance method with the optimized circuit model is valid to FE/DE capacitors.

As mentioned above, the relationship between  $G_P/\omega$  and  $f$  can be utilized to quantitatively extract the properties of interface traps. Note that  $G_P$  in (2) is composed of two terms. For the first one, it is always equal to zero when assuming  $\omega$  to be either zero or infinity, which means there must be a peak as the red dashed line shown in Fig. 4(c). As for the second term,  $G_L/\omega$  is inversely proportional to  $f$  as the blue dotted line shown in Fig. 4(c). Here, this  $G_L$  can be obtained by measuring the leakage current of FE/DE capacitors. Although this term is important in low-frequency regimes, it can be negligible in high-frequency regimes where the peak appears. Note, this conductance of the leakage current of  $G_L$  from top to the bottom electrode does not contribute to a conductance peak. Consequently, by adding these two together, the final curve of  $G_P/\omega$  versus  $f$  decreases first and then presents a peak with the generally increasing frequency, as the solid black line depicted in Fig. 4(c).

When carrying out the conductance measurement, a series of small ac signals with frequency changing over a wide range

is applied to the FE/DE capacitors already biased at a constant voltage. Interfacial charges are resonances with the small ac signal at a certain frequency and then present a peak in the black solid line shown in Fig. 4(c). As (7) formulated, this peak value  $(G_P/\omega)_{\max}$  provides the information of  $D_{it}$  ( $D_{it} \equiv C_{it}/q$ ) at the FE/DE interface. And  $\tau_{it}$  can be obtained from the corresponding frequency  $\omega_{\text{peak}}$  where the peak occurs using (8)

$$\left(\frac{G_P}{\omega}\right)_{\max} = \frac{C_{DE}^2}{2(C_{FE} + C_{DE})C_A} C_{it} \quad (7)$$

$$\omega_{\text{peak}} = \frac{C_{FE} + C_{DE} + C_{it}}{(C_{FE} + C_{DE})\tau_{it}}. \quad (8)$$

However, a random distribution of discrete charges at the FE/DE interface makes the situation complicated and causes a deviation from the ideal case. With a nonuniform distribution of localized charges over the FE/DE interfacial plane, band bending fluctuation-induced  $\tau_{it}$  dispersion should be considered. The Gaussian distribution is the most common statistical distribution characterized by only mean value and variance, which can be applied to describe this  $\tau_{it}$  dispersion. Then, (2) for  $D_{it}$  extraction becomes

$$\frac{G_P}{\omega} = \int_{-\infty}^{+\infty} \frac{(\omega\tau_{it})C_{DE}^2C_{it}}{(\omega\tau_{it})^2(C_{FE} + C_{DE})^2 + C_A^2} P(\tau) d\tau + \frac{G_L}{\omega} \quad (9)$$

where  $P(\tau)$  is a probability distribution of  $\tau_{it}$  given by

$$P(\tau) = \frac{1}{\sqrt{2\pi\sigma_{it}^2}} \exp\left(-\frac{(\tau - \bar{\tau}_{it})^2}{2\sigma_{it}^2}\right) \quad (10)$$

where  $\sigma_{it}$  is the standard deviation of  $\tau_{it}$  and  $\bar{\tau}_{it}$  is the mean value of  $\tau_{it}$ . Finally,  $D_{it}$  and  $\tau_{it}$  at the FE/DE interface can be obtained by fitting the measured  $G_L$ ,  $G_P$ , and  $C_P$  with the theoretical model given by (9) and (10).

It should be noted that the branch of  $R_{it}$  and  $C_{it}$  in Fig. 4(a) is connected to  $C_{FE}$  in parallel rather than  $C_{DE}$ , because this scheme has the best fit to experimental data (shown in Section III-C). This circuit scheme reveals that the FE/DE interface traps are most likely to be intrinsically related to the FE layer. Meanwhile, another four schemes were also attempted: 1) connecting branch of  $R_{it}$  and  $C_{it}$  to  $C_{DE}$ ; 2) only considering  $G_L$  through DE layer; 3) only considering  $G_L$  through FE layer; and 4) separating  $G_L$  into two components including one through DE layer and another through FE layer. By modeling and calculating, all these schemes were examined to be against the experimental observations, which cannot follow the trend of  $C_P$  and even contribute to a peak of  $G_P/\omega$ .

### C. Extraction of $D_{it}$ and $\tau_{it}$

Fig. 5(a) plots the measurement result of  $G_P/\omega$  as a relationship to log frequency with negative bias voltages applied. And the results under positive bias voltage are shown in Fig. 5(b). Clear conductance peaks with different peak values are observed at different bias voltages, which can be used for the extraction of  $D_{it}$  and  $\tau_{it}$ . And this conductance method has also been applied to the control samples, the metal/ferroelectric/metal capacitors with pure HZO film and metal/insulator/metal capacitors with pure  $Al_2O_3$  film. There is no conductance peak observed in these two capacitors,

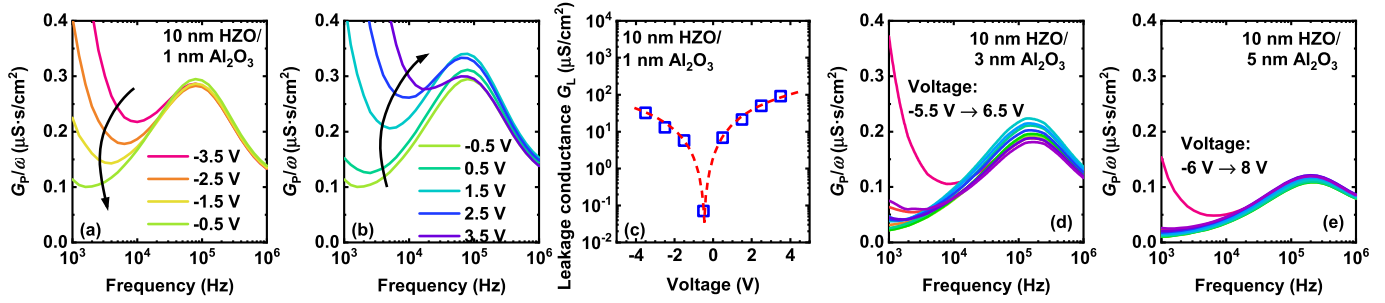


Fig. 5. Experimental results of the  $G_P/\omega$  versus  $\log f$  measured at different (a) negative and (b) positive bias voltages in the 10-nm HZO/1-nm  $\text{Al}_2\text{O}_3$  capacitor. (c) Leakage conductance  $G_L$  of 10-nm HZO/1-nm  $\text{Al}_2\text{O}_3$  under different bias voltages. (d) Experimental results of the  $G_P/\omega$  versus  $\log f$  at different voltages with 1 V/step, for the HZO/ $\text{Al}_2\text{O}_3$  capacitors with the DE thickness of (d) 3 and (e) 5 nm.

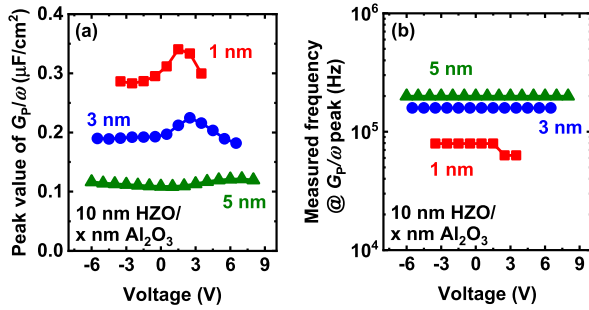


Fig. 6. Summarized (a) conductance peak values  $(G_P/\omega)_{\max}$  and (b) measured frequencies at peaks under different bias voltages for the HZO/ $\text{Al}_2\text{O}_3$  capacitors with different thicknesses of  $\text{Al}_2\text{O}_3$ .

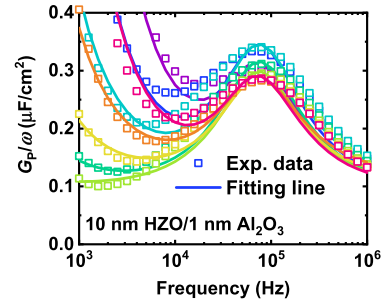


Fig. 7. Experimental data (squares) and fitting results (solid lines) of the conductance curve as a function of  $\log$  frequency taken from the 10-nm HZO/1-nm  $\text{Al}_2\text{O}_3$  capacitor. The bias voltage ranges from  $-3.5$  to  $3.5$  V. Different color corresponds to that in Fig. 5.

illustrating the peak of  $G_P/\omega$  in Fig. 5 is induced by the FE/DE interface rather than FE or DE layer itself. Besides, at low frequency of less than 10 kHz, the measured  $G_P/\omega$  in Fig. 5(a) and (b) decreases as the absolute value of the negative bias voltage decreases. However, the measured  $G_P/\omega$  increases with the increasing positive bias. This is due to the impact of  $G_L$  term in (9). The changing tendency of  $G_L$  is consistent with the measured  $I-V$  properties of this capacitor, as shown in Fig. 5(c). Through calculation, the peak value of  $G_P/\omega$  has been verified to be hardly affected by this  $G_L$  term since the measured  $G_L$  is small and the  $\omega_{\text{peak}}$  is large.

Furthermore, the measured  $G_P/\omega$  as a function of  $\log$  frequency is shown in Fig. 5(d) and (e) for the HZO/ $\text{Al}_2\text{O}_3$  capacitors with 3- and 5-nm  $\text{Al}_2\text{O}_3$ , respectively. Fig. 6(a) and (b) summarizes these measured peak information of  $(G_P/\omega)_{\max}$  and  $\omega_{\text{peak}}$  with an evolution of bias voltage, respectively. It is observed that  $(G_P/\omega)_{\max}$  decreases and  $\omega_{\text{peak}}$  increases with the increasing  $\text{Al}_2\text{O}_3$  thickness, suggesting different charge trapping behaviors. There are obvious peaks in the voltage distributions of  $(G_P/\omega)_{\max}$  appearing around coercive voltages while  $\omega_{\text{peak}}$  almost keeps at the same value for a given DE thickness.

Fig. 7 gives an example of fitting results in the 10-nm HZO/1-nm  $\text{Al}_2\text{O}_3$  capacitor by using the measured  $(G_P/\omega)_{\max}$  and  $G_L$ . The experimental data at different bias voltages exhibit good agreement with the theoretically fitting lines calculated by (9) and (10), which are favorable for the extraction of  $D_{\text{it}}$  and  $\tau_{\text{it}}$ . This also verifies the validity of this technique for quantitative trap characterization at the FE/DE interface. Finally, the voltage distribution of  $D_{\text{it}}$  at different

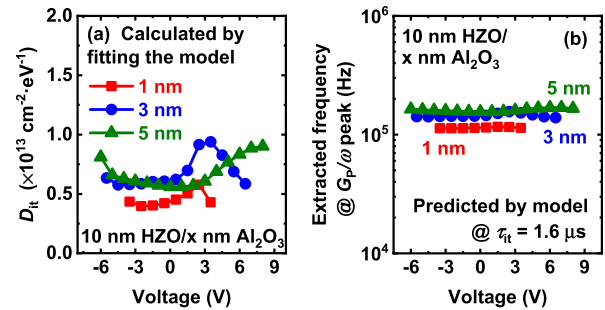


Fig. 8. (a) Calculated  $D_{\text{it}}$  of the HZO/ $\text{Al}_2\text{O}_3$  capacitors with different  $\text{Al}_2\text{O}_3$  thicknesses. (b) Peak frequency values predicted by the model when  $\tau_{\text{it}}$  is around  $1.6 \mu\text{s}$ .

$\text{Al}_2\text{O}_3$  thicknesses are extracted and summarized in Fig. 8(a). It shows  $D_{\text{it}}$  is at the order of  $\sim 4 \times 10^{12}$  to  $10^{13} \text{ cm}^{-2} \cdot \text{eV}^{-1}$  and  $D_{\text{it}}$  increases obviously around coercive voltage, suggesting a strong charge trapping during polarization switching. The small discrepancy of  $D_{\text{it}}$  with different  $\text{Al}_2\text{O}_3$  thicknesses illustrates that the thickness of the DE layer has little impact on the charge trapping, which demonstrates the assumption of intrinsic relationships between FE/DE interface traps and FE layer, mentioned in Section III-B.

It should be noted that this extracted  $D_{\text{it}}$  is the interface trap response to the small signals. It is fundamentally different from the charge density induced by ferroelectric polarization switching with large signal in [20] and [21]. The FE/DE capacitor has been biased at a constant voltage during the conductance measurement and the polarization switching has already finished. Moreover, the measured voltage distribution

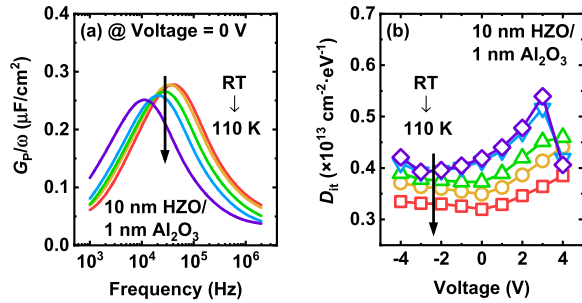


Fig. 9. (a) Measured  $G_p/\omega$  with the relationship to frequency in log scale curves of the 10-nm HZO/1-nm  $\text{Al}_2\text{O}_3$  capacitor at different temperatures ranging from RT to 110 K. (b) Extracted  $D_{it}$  distributions under different bias voltages at low temperatures.

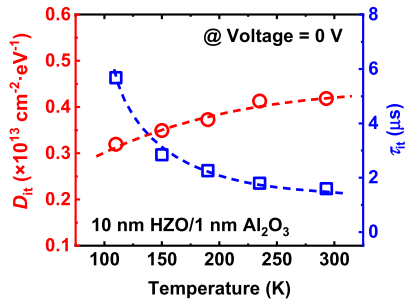


Fig. 10. Temperature-dependent  $D_{it}$  and  $\tau_{it}$  at zero bias voltage ranging from RT to 110 K. Charge injection and trap response are suppressed at low temperatures.

of  $D_{it}$  corresponds to the trap density at different polarization states. By integrating them into the energy band during polarization switching, almost the same result with the data in [20] and [21] can be obtained. This accordance verifies that it is reasonable to adopt the conductance method to FE/DE stacks for  $D_{it}$  and  $\tau_{it}$  extraction.

Fig. 8(b) shows the extracted  $\omega_{peak}$  by the proposed model when assuming  $\tau_{it}$  of  $\sim 1.6 \mu\text{s}$ , which shows an approximative result with the measured in Fig. 6(b). Here,  $\tau_{it}$  is assumed at the same value for FE/DE stacks with different  $\text{Al}_2\text{O}_3$  thicknesses since  $R_{it}$  and  $C_{it}$  are mainly related to the FE layer in the equivalent circuit model for the conductance method, as shown in Fig. 4(a).

It also indicates that the charging/discharging process at the FE/DE interface could be effectively suppressed if the measurement frequency is up to more than 1 MHz, being consistent with the results in Fig. 3.

#### D. Behaviors of FE/DE Interface Traps at Low Temperature

To further understand the behaviors of FE/DE interface traps, the conductance method was also applied to 10-nm HZO/1-nm  $\text{Al}_2\text{O}_3$  capacitors at low temperatures. Fig. 9(a) shows the experimental  $G_p/\omega$  with a relationship to log frequency at zero bias voltage measured from RT to 110 K. Fig. 9(b) shows the extracted voltage-dependent  $D_{it}$  at different temperatures. The peak value and frequency at peak both decrease with the decreasing measurement temperature.

As summarized in Fig. 10,  $D_{it}$  at the FE/DE interface is smaller at lower temperatures, due to a weaker charge

trapping/detrapping process, which suggests the reduction of leakage current through the DE layer and the suppression of trap response at the FE/DE interface. This phenomenon also agrees well with  $C-V$  measurement results in Fig. 3(b). In addition,  $\tau_{it}$  was extracted and shown as the blue squares in Fig. 10. As the temperature decreases, a larger  $\tau_{it}$  can be found. This can be attributed to the fact that charge injection is inhibited and trap response is slowed down.

#### IV. CONCLUSION

In conclusion, the FE/DE interface is experimentally investigated in a simple capacitor structure using the conductance method with an improved circuit model. The components and connection of the circuit model for the conductance method are analyzed in detail, and the nonuniform trap distribution is also taken into consideration. With the proposed measurement technique, the  $D_{it}$  at different static polarization states is obtained to be  $\sim 4 \times 10^{12}$  to  $10^{13} \text{ cm}^{-2} \cdot \text{eV}^{-1}$ , indicating a critical role of charge trapping at the FE/DE interface during the operation of FE/DE stack. Besides, the smaller  $D_{it}$  and larger  $\tau_{it}$  at low temperatures confirm the suppression of trap response. This conductance method provides a new approach and possible new insights to understand the mechanism of NC-FETs and Fe-FETs operations and their reliability degradations.

#### REFERENCES

- [1] J. Müller *et al.*, "Ferroelectric  $\text{Zr}_{0.5}\text{Hf}_{0.5}\text{O}_2$  thin films for nonvolatile memory applications," *Appl. Phys. Lett.*, vol. 99, no. 11, 2011, Art. no. 112901, doi: [10.1063/1.3636417](https://doi.org/10.1063/1.3636417).
- [2] T. P. Ma and J.-P. Han, "Why is nonvolatile ferroelectric memory field-effect transistor still elusive?" *IEEE Electron Device Lett.*, vol. 23, no. 7, pp. 386–388, Jul. 2002, doi: [10.1109/LED.2002.1015207](https://doi.org/10.1109/LED.2002.1015207).
- [3] S. Müller *et al.*, "From MFM capacitors toward ferroelectric transistors: Endurance and disturb characteristics of  $\text{HfO}_2$ -based FeFET devices," *IEEE Trans. Electron Devices*, vol. 60, no. 12, pp. 4199–4205, Dec. 2013, doi: [10.1109/TED.2013.2283465](https://doi.org/10.1109/TED.2013.2283465).
- [4] H. Ishiwara, T. Shimamura, and E. Tokumitsu, "Proposal of a single-transistor-cell-type ferroelectric memory using an SOI structure and experimental study on the interference problem in the write operation," *Jpn. J. Appl. Phys.*, vol. 36, no. 3S, pp. 1655–1658, 1997, doi: [10.1143/JJAP.36.1655](https://doi.org/10.1143/JJAP.36.1655).
- [5] M. Jerry *et al.*, "Ferroelectric FET analog synapse for acceleration of deep neural network training," in *IEDM Tech. Dig.*, Dec. 2017, pp. 139–142, doi: [10.1109/IEDM.2017.8268338](https://doi.org/10.1109/IEDM.2017.8268338).
- [6] S. Salahuddin and S. Datta, "Use of negative capacitance to provide voltage amplification for low power nanoscale devices," *Nano Lett.*, vol. 8, no. 2, pp. 405–410, Feb. 2008, doi: [10.1021/nl071804g](https://doi.org/10.1021/nl071804g).
- [7] K.-S. Li *et al.*, "Sub-60 mV-swing negative-capacitance FinFET without hysteresis," in *IEDM Tech. Dig.*, Dec. 2015, pp. 620–623, doi: [10.1109/IEDM.2015.7409760](https://doi.org/10.1109/IEDM.2015.7409760).
- [8] M. H. Lee *et al.*, "Ferroelectric hafnium oxide: A CMOS-compatible and highly scalable approach to future ferroelectric memories," in *IEDM Tech. Dig.*, Dec. 2016, pp. 306–309, doi: [10.1109/IEDM.2016.7838400](https://doi.org/10.1109/IEDM.2016.7838400).
- [9] M. Si *et al.*, "Steep-slope hysteresis-free negative capacitance  $\text{MoS}_2$  transistors," *Nature Nanotechnol.*, vol. 13, no. 1, pp. 24–28, Jan. 2018, doi: [10.1038/s41565-017-0010-1](https://doi.org/10.1038/s41565-017-0010-1).
- [10] W. Chung, M. Si, and P. D. Ye, "First demonstration of ge ferroelectric nanowire FET as synaptic device for online learning in neural network with high number of conductance state and  $G_{max}/G_{min}$ ," in *IEDM Tech. Dig.*, Dec. 2018, pp. 344–347, doi: [10.1109/IEDM.2018.8614516](https://doi.org/10.1109/IEDM.2018.8614516).
- [11] A. I. Khan, U. Radhakrishna, K. Chatterjee, S. Salahuddin, and D. A. Antoniadis, "Negative capacitance behavior in a leaky ferroelectric," *IEEE Trans. Electron Devices*, vol. 63, no. 11, pp. 4416–4422, Nov. 2016, doi: [10.1109/TED.2016.2612656](https://doi.org/10.1109/TED.2016.2612656).

- [12] Z. Liu, M. A. Bhuiyan, and T. P. Ma, "A critical examination of 'quasi-static negative capacitance' (QSNC) theory," in *IEDM Tech. Dig.*, Dec. 2018, p. 31, doi: [10.1109/IEDM.2018.8614614](https://doi.org/10.1109/IEDM.2018.8614614).
- [13] Y. J. Kim *et al.*, "Interfacial charge-induced polarization switching in  $\text{Al}_2\text{O}_3/\text{Pb}(\text{Zr},\text{Ti})\text{O}_3$  bi-layer," *J. Appl. Phys.*, vol. 118, no. 22, Dec. 2015, Art. no. 224105, doi: [10.1063/1.4937544](https://doi.org/10.1063/1.4937544).
- [14] F.-C. Sun, M. T. Kesim, Y. Espinal, and S. P. Alpay, "Are ferroelectric multilayers capacitors in series?" *J. Mater. Sci.*, vol. 51, no. 1, pp. 499–505, Jan. 2016, doi: [10.1007/s10853-015-9298-0](https://doi.org/10.1007/s10853-015-9298-0).
- [15] Y. J. Kim *et al.*, "Time-dependent negative capacitance effects in  $\text{Al}_2\text{O}_3/\text{BaTiO}_3$  bilayers," *Nano Lett.*, vol. 16, no. 7, pp. 4375–4381, Jul. 2016, doi: [10.1021/acs.nanolett.6b01480](https://doi.org/10.1021/acs.nanolett.6b01480).
- [16] M. Hoffmann, B. Max, T. Mittmann, U. Schroeder, S. Slesazek, and T. Mikolajick, "Demonstration of high-speed hysteresis-free negative capacitance in ferroelectric  $\text{Hf}_{0.5}\text{Zr}_{0.5}\text{O}_2$ ," in *IEDM Tech. Dig.*, Dec. 2018, pp. 727–730, doi: [10.1109/IEDM.2018.8614677](https://doi.org/10.1109/IEDM.2018.8614677).
- [17] M. A. Alam, M. Si, and P. D. Ye, "A critical review of recent progress on negative capacitance field-effect transistors," *Appl. Phys. Lett.*, vol. 114, no. 9, Mar. 2019, Art. no. 090401, doi: [10.1063/1.5092684](https://doi.org/10.1063/1.5092684).
- [18] M. Si, X. Lyu, and P. D. Ye, "Ferroelectric polarization switching of hafnium zirconium oxide in a ferroelectric/dielectric stack," *ACS Appl. Electron. Mater.*, vol. 1, no. 5, pp. 745–751, May 2019, doi: [10.1021/acsaem.9b00092](https://doi.org/10.1021/acsaem.9b00092).
- [19] K. D. Kim *et al.*, "Transient negative capacitance effect in atomic-layer-deposited  $\text{Al}_2\text{O}_3/\text{Hf}_{0.3}\text{Zr}_{0.7}\text{O}_2$  bilayer thin film," *Adv. Funct. Mater.*, vol. 29, no. 17, Apr. 2019, Art. no. 1808228, doi: [10.1002/adfm.201808228](https://doi.org/10.1002/adfm.201808228).
- [20] K. Toprasertpong, M. Takenaka, and S. Takagi, "Direct observation of interface charge behaviors in FeFET by quasi-static split C-V and Hall techniques: Revealing FeFET operation," in *IEDM Tech. Dig.*, Dec. 2019, pp. 570–573, doi: [10.1109/IEDM19573.2019.8993664](https://doi.org/10.1109/IEDM19573.2019.8993664).
- [21] J. Li, Y. Qu, M. Si, X. Lyu, and P. D. Ye, "Multi-probe characterization of ferroelectric/dielectric interface by C-V, P-V and conductance methods," in *Proc. IEEE Symp. VLSI Technol.*, Jun. 2020, pp. 44–45.
- [22] K. Ni *et al.*, "Critical role of interlayer in  $\text{Hf}_{0.5}\text{Zr}_{0.5}\text{O}_2$  ferroelectric FET nonvolatile memory performance," *IEEE Trans. Electron Devices*, vol. 65, no. 6, pp. 2461–2469, Jun. 2018, doi: [10.1109/TED.2018.2829122](https://doi.org/10.1109/TED.2018.2829122).
- [23] Y. Higashi *et al.*, "Impact of charge trapping on imprint and its recovery in  $\text{HfO}_2$  based FeFET," in *IEDM Tech. Dig.*, Dec. 2019, pp. 358–361, doi: [10.1109/IEDM19573.2019.8993472](https://doi.org/10.1109/IEDM19573.2019.8993472).
- [24] Y. Higashi *et al.*, "New insights into the imprint effect in FE- $\text{HfO}_2$  and its recovery," in *Proc. IEEE Int. Rel. Phys. Symp. (IRPS)*, Mar./Apr. 2019, pp. 1–7, doi: [10.1109/IRPS.2019.8720553](https://doi.org/10.1109/IRPS.2019.8720553).
- [25] E. H. Nicollian and A. Goetzberger, "The si-sio, interface-electrical properties as determined by the metal-insulator-silicon conductance technique," *Bell Syst. Tech. J.*, vol. 46, no. 6, pp. 1033–1055, Jul./Aug. 1967, doi: [10.1002/j.1538-7305.1967.tb01727.x](https://doi.org/10.1002/j.1538-7305.1967.tb01727.x).
- [26] V. Garcia and M. Bibes, "Ferroelectric tunnel junctions for information storage and processing," *Nature Commun.*, vol. 5, no. 1, pp. 1–12, Sep. 2014, doi: [10.1038/ncomms5289](https://doi.org/10.1038/ncomms5289).
- [27] M. Houssa *et al.*, "Trap-assisted tunneling in high permittivity gate dielectric stacks," *J. Appl. Phys.*, vol. 87, no. 12, pp. 8615–8620, Jun. 2000, doi: [10.1063/1.373587](https://doi.org/10.1063/1.373587).